Quality Enhancement in Holographic Imaging by Background Property Estimation

Hailun Wu, *Student Member, IEEE*, Kruti Patel, and Reza K. Amineh, Senior *Member, IEEE*

***Abstract*— In this communication, we propose a technique to enhance the quality of images obtained from holographic microwave imaging. It is based on estimating the electrical properties of the background medium. To accomplish that, background properties to be estimated are assumed to be within a pre-known range. Then, two sets of frequencies are employed in wideband holographic imaging and images are reconstructed from each set and for assumed property values within the pre-determined range. An error is calculated according to the differences between the two sets of images. The error is expected to be minimum at the true values of the background medium's properties. The estimated properties, in turn, are used to reconstruct images with the best quality. The validity of the proposed technique is demonstrated via simulation and experimental results.**

***Index Terms*— Image reconstruction, microwave holography, near-field microwave imaging.**

I. Introduction

The relatively long wavelength of microwave and millimeter waves allows for penetration inside dielectric bodies where visible light cannot reach. Based on this property, various techniques have been proposed to harness the ability of microwaves for two-dimensional (2D) and three-dimensional (3D) imaging in a wide variety of applications such as biomedical imaging (e.g., see [1][2]), concealed weapon detection (e.g., see [3][4]), wall or through-the-wall imaging (e.g., see [5][6]), nondestructive testing (NDT) (e.g., see [7][8]), etc. While some of these applications are still in research phase, others have been developed, commercialized, and employed in practice. A prominent and mature application is millimeter wave security screening of the passengers in the airports [9]-[10]. There, holographic imaging has been very successful in providing fast and robust 3D images.

The recent progress in the field of holographic microwave imaging can be divided into two separate paths: indirect holography [11]-[13] and direct holography [9]-[10]. The indirect microwave holography has the most resemblance to optical holography in terms of recording of a hologram. The major advantage of indirect holography is that the phase information is mathematically recovered from low-cost intensity-only scalar microwave measurements. This simplifies the hardware implementation and reduces the cost of the imaging system. The direct holographic microwave imaging techniques, however, use RF circuitry or vector network analyzer (VNA) to record both the magnitude and phase of the back-scattered waves directly. As the direct holographic algorithms developed, their resemblance to synthetic aperture radar (SAR) based imaging methods became evident. Currently, the terms SAR imaging and direct microwave holography are being used to refer to reconstruction approaches that are mathematically very similar, in particular, for far-field imaging applications. By collecting wideband data, 3D imaging reconstruction is possible using direct holographic imaging techniques.

To alleviate issues regarding the far-field approximations and interpolation in k-space in far-field direct holographic imaging, near-field holographic imaging techniques have been proposed that solve the inverse scattering problem via the use of forward and inverse Fourier transforms (FT) and solution of linear systems of equations. Such near-field holographic imaging techniques can be implemented employing wideband data [14]-[16] or single frequency data [17].

In microwave imaging, typically, it is assumed that the background medium is a homogenous medium with pre-known values of electrical permittivity ε and electrical conductivity σ. However, in practice, the electrical properties of the background medium may not be exactly known. Uncertainties in knowing their exact values lead to degradation of the image quality in microwave imaging of hidden objects. This necessitates the development of new algorithms to estimate the effective values of ε and σ so that the image reconstruction can be implemented with the right property values.

In this communication, for the first time, we present a technique to estimate the electrical properties of the background medium in holographic imaging. The proof-of-concept simulation and experimental results demonstrate the validity of the proposed technique to enhance the quality of the reconstructed images.

II. Theory

In this section, we briefly review the theory of near-field holographic imaging and then proceed with proposing the technique for background property estimation.

A. Wideband Holographic Imaging

Fig. 1 illustrates a typical microwave holographic imaging setup based on collection of back-scattered data over a rectangular aperture. It consists of a transmitter antenna that illuminates the object with wideband microwave power and moves over a rectangular aperture. At each position (x, y), the scattered field is recorded by the same antenna or a receiver antenna that moves together with the transmitter antenna. By subtracting the responses recorded without the presence of the objects from the responses recorded with the presence of the objects, the back-scattered fields only due to the objects are obtained and denoted by $E^{sc}(x,y,f)$. These are referred to as *calibrated responses*. By collecting data at N_f frequencies, the contrast functions for the objects under test (OUT) $c_i(x,y)$ are reconstructed over $z = z_i$ planes, where $i = 1,\ldots, N_z$.

In near-field holographic imaging [17], using the convolution theory, first the point-spread function (PSF) of the system is measured or simulated *a priori*, assuming that the type and properties of background medium is completely known. In practice, collection of PSFs can be achieved by recording the responses for point-wise objects called calibration objects (COs). These are the smallest objects with the largest contrast that can be measured by the system

The authors are with the Department of Electrical and Computer Engineering, New York Institute of Technology, New York, NY 10023, United States (e-mail: hwu28@nyit.edu; rkhalaja@nyit.edu; kpate213@nyit.edu)

and approximately represent an impulse function (Dirac delta function) as an input to the imaging system. We denote the PSF recorded for the $z = z_i$ plane at frequency f as $E_i^{sc,co}(x,y,f)$.

As shown in [17], the total response $E^{sc}(x,y,f)$ measured by the receiver antenna due to the OUTs is written as the superposition of responses produced by objects over all planes:

$$E^{sc}(x,y,f) = \sum_{i=1}^{N_z} E_i^{sc}(x,y,f) = \sum_{i=1}^{N_z} E_i^{sc,co}(x,y,f) *_x *_y c_i(x,y) \tag{1}$$

As discussed above, in (1), $E_i^{sc,co}(x,y,f)$ functions are measured or simulated *a priori* using COs one at a over each $z = z_i$ plane. Also, $E^{sc}(x,y,f)$ functions are known from the measurement of the OUT's responses. In order to estimate the OUT's contrast functions $c_i(x,y)$, the scattered waves are acquired at multiple frequencies, f_l, $l = 1,\ldots, N_f$. Then, re-writing (1) at all frequencies leads to the following system of equations:

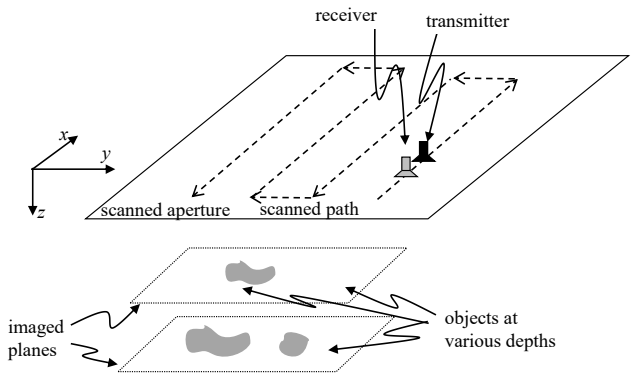

Fig. 1. Illustration of a wideband 3D microwave holographic imaging setup.

$$\begin{cases} E^{sc}(x,y,f_1) = \sum_{i=1}^{N_z} E_i^{sc,co}(x,y,f_1) *_x *_y c_i(x,y) \\ \vdots \\ E^{sc}(x,y,f_{N_f}) = \sum_{i=1}^{N_z} E_i^{sc,co}(x,y,f_{N_f}) *_x *_y c_i(x,y) \end{cases} \tag{2}$$

To solve for unknowns $c_i(x,y)$, we can take two-dimensional (2D) Fourier transform (FT) with respect to x and y variables, with k_x and k_y denoting the Fourier variables, for all the equations in (2) to obtain:

$$\begin{cases} \tilde{\tilde{E}}^{sc}(k_x,k_y,f_1) = \sum_{i=1}^{N_z} \tilde{\tilde{E}}_i^{sc,co}(k_x,k_y,f_1)\tilde{\tilde{c}}_i(k_x,k_y) \\ \vdots \\ \tilde{\tilde{E}}^{sc}(k_x,k_y,f_{N_f}) = \sum_{i=1}^{N_z} \tilde{\tilde{E}}_i^{sc,co}(k_x,k_y,f_{N_f})\tilde{\tilde{c}}_i(k_x,k_y) \end{cases} \tag{3}$$

where $\tilde{\tilde{E}}^{sc}(k_x,k_y,f_l)$, $\tilde{\tilde{E}}_i^{sc,co}(k_x,k_y,f_l)$ and $\tilde{\tilde{c}}_i(k_x,k_y)$ are the 2D FTs of the functions $E^{sc}(x,y,f_l)$, $E_i^{sc,co}(x,y,f_l)$ ($l = 1,\ldots,N_f$), and $c_i(x,y)$, respectively. At each spatial frequency pair (k_x, k_y), we solve a system of equations as in (3). Once this process is implemented for all variations of (k_x, k_y), $\tilde{\tilde{c}}_i(k_x,k_y)$ will be obtained. Then, a 2D image at each $z = z_i$ plane is reconstructed by taking inverse 2D FT of $\tilde{\tilde{c}}_i(k_x,k_y)$. Finally, the normalized 2D images of the OUTs at all N_z planes $|c_i(x,y)|/M$ are obtained, where M is the maximum of $|c_i(x,y)|$ for all planes and $|c_i(x,y)|$ is the magnitude of $c_i(x,y)$. All 2D slice images can be put together to form a 3D image of the OUTs.

In the previous works on holographic imaging (see [9], [15], and [16]), range and cross-range resolution limits have been discussed in detail. For instance, it has been shown in [9] that due the use of far field approximations, the resolution will be restricted by the well-known diffraction limit. Besides, it has been shown in [15] and [16] that higher resolutions can be achieved in the near field imaging since the evanescent waves spectrum can be partially measured.

B. Estimation of Background Medium's Properties

In the holographic technique described above, we assumed that the type (properties) of the background medium is known so that the relevant PSFs can be employed in the image reconstruction process. However, in practice, there might be uncertainty in knowing the exact background medium and its properties which leads to image reconstruction errors. To estimate the effective electrical properties of the background medium and improve the quality of reconstructed images, we propose an algorithm with the following steps:

1) Divide the responses acquired at all frequencies f_l, $l = 1,\ldots, N_f$ into two sets: Set 1 includes responses at frequencies f_o, where o is an odd integer number as $o = 1,3,\ldots,N_o$, where $N_o \le N_f$ and Set 2 includes responses at frequencies f_e, where e is an even integer number as $e = 2,4,\ldots,N_e$, where $N_e \le N_f$.
2) Choose a range of possible values for ε and σ as $\varepsilon = \varepsilon_m$, $m = 1,\ldots,N_\varepsilon$ and $\sigma = \sigma_n$, $n = 1,\ldots, N_\sigma$.
3) For each (ε_m, σ_n) pair, use Set 1 and Set 2 responses and apply holographic imaging algorithm on them separately to obtain images, $I_1^{(m,n)}(x,y,z_i)$ and $I_2^{(m,n)}(x,y,z_i)$, respectively.
4) For (ε_m, σ_n) pair in step 3, the difference between the 3D images $I_1^{(m,n)}$ and $I_2^{(m,n)}$ is evaluated, for example, via computing the total error E_T as the sum of 2-norm of the difference between the images at each depth z_i as
$$E_T(m,n) = \sum_{i=1}^{N_z} \| I_1^{(m,n)}(x,y,z_i) - I_2^{(m,n)}(x,y,z_i) \| \tag{4}$$
where $\|\cdot\|$ is the 2-norm operator.
5) The true values of (ε, σ) are estimated as (ε_m, σ_n) for which $E_T(m,n)$ is the lowest. This indicates that the images obtained from Set 1 and Set 2 responses are the most consistent when they are reconstructed with the true values of electrical properties.

Fig. 2 shows the flowchart of the algorithm for background property estimation summarizing the main steps discussed above.

III. Results

In this section, we present simulation and experimental results to validate the performance of the proposed background property estimation algorithm.

A. Simulation Results

The simulation study is performed employing FEKO software which is a high frequency electromagnetic simulation tool based on method of moments. Simulations are performed in the frequency range of 3 GHz to 10 GHz with steps of 0.5 GHz. OUTs are five spheres with radii of $r = 2$ mm and properties of $\varepsilon_r = 20$ and $\sigma = 1$

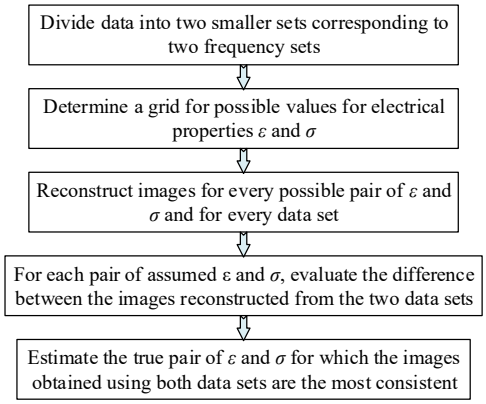

Fig. 2. Flowchart of estimating electrical properties of the background medium.

S/m. They are placed in a background medium with properties of $\varepsilon_r = 6$ and $\sigma = 0.5$ S/m at the positions of $(0,0,-50)$, $(\pm 10,0,-60)$, and $(0,\pm 10,-60)$ as shown in Fig. 3. A resonant dipole antenna is scanning at h = 10 mm over a rectangular aperture with size of 10λ, where λ is the wavelength at the center frequency of 6.5 GHz, and with steps of 0.25λ. The images are reconstructed over planes of $z_1 = -30$ mm, $z_2 = -40$ mm, $z_3 = -50$ mm, and $z_4 = -60$ mm. The collected responses are separated in two sets. One of them consists of frequency range of 3 GHz to 10 GHz with steps of 1 GHz while the

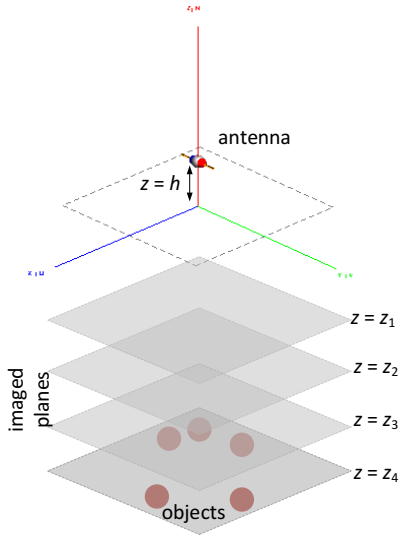

Fig. 3. Simulation setup in FEKO.

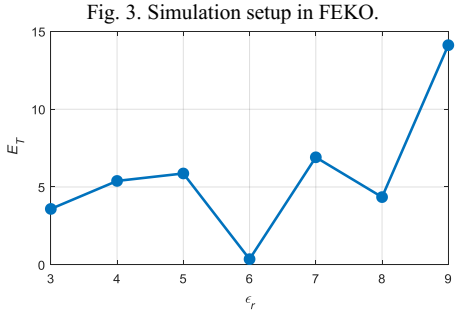

Fig. 4. Total error versus to the assumed permittivity values.

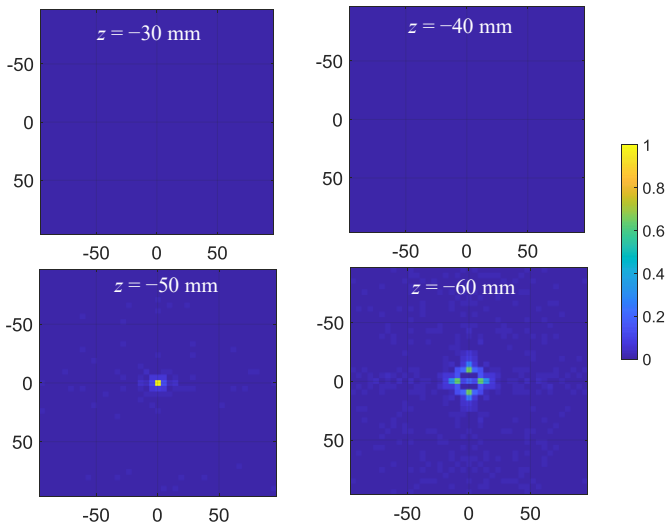

Fig. 5. Reconstructed images with the right relative permittivity value of 6. Horizontal axis: x (mm), vertical axis: y (mm)

other one consists of frequency range of 3.5 GHz to 9.5 GHz with steps of 1 GHz. Conductivity σ of the background medium is assumed to be known and the unknown permittivity ε_r is assumed to be within the range of 3 to 9. Using the *calibrated responses*, we reconstruct images with the collected PSFs corresponding to ε_r in the range of 3 to 9 with a step of 1. By applying the proposed algorithm, we obtain E_T values shown in Fig. 4 for which the minimum appears at $\varepsilon_r = 6$ which is the true value of background medium's permittivity. This validates the proposed technique. Thus, images are reconstructed with the PSFs at $\varepsilon_r = 6$. Fig. 5 shows the reconstructed images when using the PSFs corresponding to the right permittivity value of $\varepsilon_r = 6$. The OUTs are reconstructed well at the true positions at each plane.

B. Experimental Results

To validate the property estimation technique, we also conduct some experiments. Fig. 6(a) shows the experimental setup including: material under test (MUT), two stepper motors for positioning along the x and y axes, Arduino Uno board with Adafruit motor shield v2.3 for controlling motors via PC, an ultrawide band (UWB) antenna manufactured by SMAKN [18] operating from 2.8 GHz to 11 GHz, and an Anritsu Shockline vector network analyzer (VNA) model MS46322B. We use three types of MUTs as shown in Fig. 6(b) with size of 30 cm × 30 cm. They include hardwood, foam which makes up ceiling tiles, and medium-density fiberboard (MDF). They are expected to have relative permittivities in the range of 1 to 3. Fig. 6(c) shows the UWB antenna placed inside a metal cavity with size of 6 cm × 5.5 cm × 4 cm for directing the microwave power toward the MUTs and reducing backward interferences. Please note that, this radiating structure may not be optimal for imaging and is only used for quick proof-of-concept experiments. During the tests, MUT is stationary while antenna is scanned by the positioning system. One of the motors moves the antenna along x axis from 0 to 23 cm in 40 steps and the other one moves it along y axis from 0 to 17 cm in 30 steps. By using these two motors, raster scanning is performed to cover an aperture of size 23 cm × 17 cm.

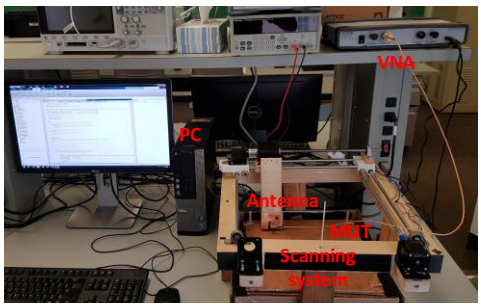

(a)

(b)

(c)

Fig. 6. (a) Experimental setup, (b) MUTs, and (c) UWB antenna.

We implement imaging over two depths of 14 mm and 42 mm deep inside these MUTs. Due to the different thicknesses of each material's sheet, we stack different number of layers of each MUT to compose the required depths. Thin copper plates with size of 4 cm × 2.5 cm are used as objects to be imaged. For each MUT, two of the objects are placed around the origin at the first depth of 14 mm with an approximate center-to-center distance of 8 cm between them. Another object is placed approximately at the origin at the depth of 42 mm.

First, we collect PSFs for all the MUTs and for the above-mentioned depths, i.e., 14 mm and 42 mm, by placing one object at a time at the corresponding depth and obtain *calibrated responses*. Then, *calibrated responses* for the objects placed at 14 mm and 42 mm are collected for each MUT. Based on the proposed technique, all the measurements are implemented at two sets of frequencies. The first set has 20 frequencies uniformly distributed over the range of 3 GHz to 8 GHz. The second set has 20 frequencies uniformly distributed over the range of 3.5 GHz to 7.5 GHz. We first try to employ these two sets of frequencies to reconstruct two sets of images and calculate the error as mentioned in section II when using PSFs measured for the same MUT and PSFs measured for the two other MUTs. Table I shows the calculated errors. It is observed that when using the PSFs corresponding to the same MUT, the error is minimum confirming the validity of the proposed algorithm.

Figs. 7(a)-(c) shows the reconstructed images when using the right PSFs for each MUT. It is observed that the objects are reconstructed well in their true positions. Two objects are reconstructed well at the depth of 14 mm and one object is reconstructed well at the depth of 42 mm for all the MUTs. Due to the slight differences in the placement of the objects in each experiment, the reconstructed images of the objects also differ slightly. The reason for noise in Figs. 7(a)-(c) could be the small gaps between layers of MUTs (which is hard to eliminate), random small mechanical ripples of the antenna during each scan, and electromagnetic interferences (EMI). We adjusted the maximum values of Fourier variables k_x and k_y to reduce the high frequency noise. Besides, we apply the image guided filtering [19] in MATLAB using *imguidedfilter* function to further reduce the background artifacts in the images. This method performs edge-preserving smoothing.

Fig. 7(d) shows the reconstructed images of objects inside the foam using PSFs corresponding to MDF. It is observed that two objects can be reconstructed on the plane with depth of $z = -14$ mm but the level of background artifacts has slightly increased and the cross-range resolution has slightly degraded (the bright spots due to the objects appear slightly wider). Besides, the single object on the plane $z = -42$ mm cannot be reconstructed at all. Overall, it is observed that when the assumed background property is not right, OUTs are not reconstructed well and the image quality degrades.

TABLE I
TOTAL ERROR (E_T) WHEN RECONSTRUCTING IMAGES WITH VARIOUS PSFS FOR THE THREE MEASURED MATERIALS

Material	PSF for MDF	PSF for Foam	PSF for Wood
MDF	4.58	10.97	11.77
Foam	2.51	1.50	2.92
Wood	1.25	3.27	1.00

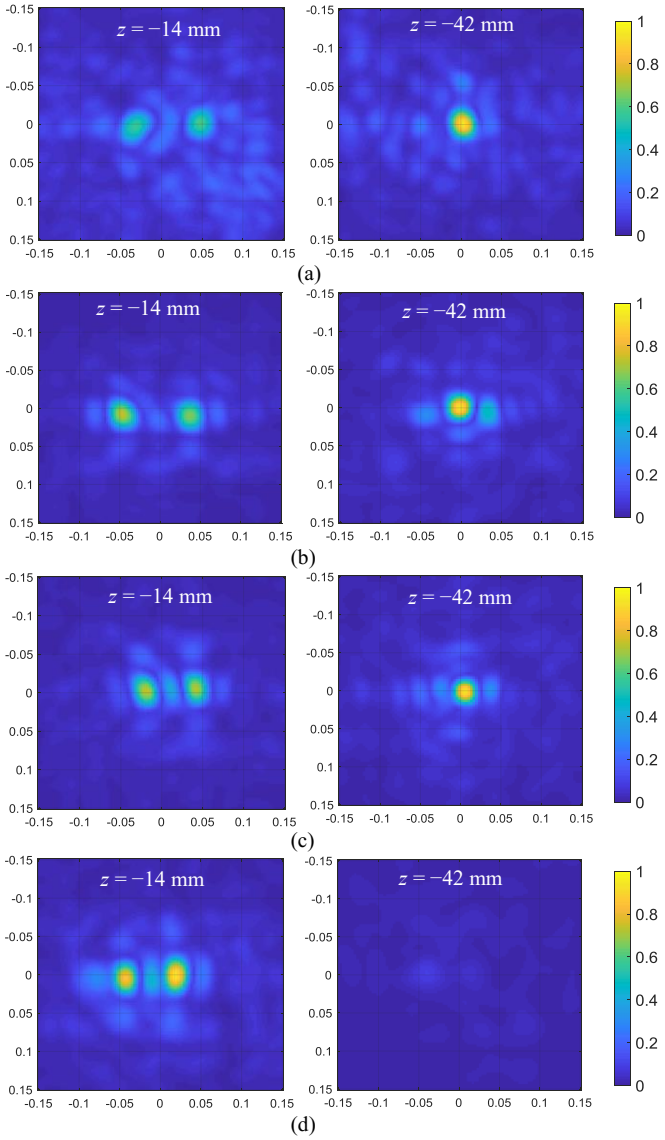

Fig. 7. Reconstructed images for each MUT: (a) MDF using PSFs corresponding to MDF, (b) wood using PSFs corresponding to wood, (c) foam using PSFs corresponding to foam, and (d) foam using PSFs corresponding to MDF. Horizontal axis: x (mm), vertical axis: y (mm).

IV. CONCLUSION

In this communication, a technique for background medium's dielectric property estimation is proposed base on the microwave holographic imaging. This technique is based on determining a possible range of values for the properties ε and σ, and at each

assumed property pair (ε, σ) within that range, comparing two sets of images obtained from the collected data at two frequency sets. This comparison is performed via computing a total error between the reconstructed images. The error is minimum at the estimated values of the dielectric properties ε and σ. Simulation and experimental studies demonstrated the validity of the proposed technique. It can be employed in various 3D imaging applications, in particular, in imaging of hidden objects (in homogeneous media or behind the walls), to enhance the quality of the reconstructed images.

In general, when the employed PSFs do not correspond to the true MUT, the matrix of coefficients for the system of equations in (3) is not accurate. This leads to errors in the solutions and can potentially degrade the image quality in both range and cross-range directions. In this study, we realized that when the utilized PSFs are for a medium with large difference in properties with respect to the MUT, both range and cross-range resolutions degrade drastically. But, when the utilized PSFs are for a medium, with small difference in properties with respect to the MUT, the objects can be localized on the right range positon but with poorer cross-range resolution. Besides, the use of more frequency data would alleviate the degradation due to the use of inaccurate PSFs and, overall, the image reconstruction process is more prone to errors (due to the use of inaccurate PSFs) for imaging of smaller objects.

Please note that applying this method to underground imaging where the background media is inhomogeneous (dielectric property changes versus depth) or where the background medium is composed of multi-layers with various dielectric properties requires further investigations. In such scenarios, the variation of dielectric properties along the depth (in underground imaging) and the thickness of layers (in imaging of layered media) need to be estimated which significantly adds to the complexity of the property estimation procedure. Such studies would be the subject of our future works.

ACKNOWLEDGMENT

This project has been supported by US national science foundation (NSF), award No. 1920098, and New York Institute of Technology's (NYIT) Institutional Support for Research and Creativity (ISRC) Grants.

REFERENCES

[1] N. K. Nikolova, "Microwave near-field imaging of human tissue and its applications to breast cancer detection," *IEEE Microwave Mag.*, vol. 12, no. 7, pp. 78–94, Dec. 2011.

[2] R. Chandra, H. Zhou, I. Balasingham, and R. M. Narayanan, "On the opportunities and challenges in microwave medical sensing and imaging," *IEEE Trans. on Biomed. Eng.*, vol. 62, no. 7, pp. 1667–1682, Jul. 2015.

[3] R. Appleby and H. B. Wallace, "Standoff detection of weapons and contraband in the 100 GHz to 1 THz region," *IEEE Trans. on Antennas and Propag.*, vol. 55, pp. 2944–2956, 2007.

[4] M. C. Kemp, "Millimetre wave and terahertz technology for the detection of concealed threats - a review," *Proc. of SPIE*, vol. 6402, 2006.

[5] K. M. Yemelyanov, N. Engheta, A. Hoorfar, and J. A. McVay, "Adaptive polarization contrast techniques for through-wall microwave imaging applications," *IEEE Trans. on Geoscience and Remote Sensing*, vol. 47, no. 5, pp. 1362–1374, May 2009.

[6] Y. Bao, M. T. Ghasrt, K. Yingt, G. Chen, and R. Zoughi, "Microwave synthetic aperture radar imaging for nondestructive evaluation of mechanically stabilized earth walls," *Materials Evaluation*, pp. 177–184, Feb. 2017.

[7] R. Zoughi, *Microwave Non-Destructive Testing and Evaluation*. Kluwer Academic Publishers, 2000.

[8] S. Kharkovsky and R. Zoughi, "Microwave and millimeter wave nondestructive testing and evaluation - Overview and recent advances," *IEEE Instr. and Meas. Mag.*, vol. 10, no. 2, pp. 26–38, Apr. 2007.

[9] M. Sheen, D. L. McMakin, and T. E. Hall, "Three-dimensional millimeter-wave imaging for concealed weapon detection," *IEEE Trans. on Microw. Theory and Tech.*, vol. 49, no. 9, pp. 1581–1592, Sep. 2001.

[10] D. M. Sheen, D. L. McMakin, and T. E. Hall, Near-field three-dimensional radar imaging techniques and applications," *Applied Optics*, vol. 49, no. 19, pp. E83–E93, Jun. 2010.

[11] D. Smith, O. Yurduseven, B. Livingstone, and V. Schejbal, "Microwave imaging using indirect holographic techniques," *IEEE Antennas and Propag. Mag.*, vol. 56, no. 1, pp. 104–117, 2014.

[12] M. Elsdon, O. Yurduseven, and D. Smith, "Early stage breast cancer detection using indirect microwave holography," Prog. Electromag. Res., vol. 143, pp. 405–419, 2013.

[13] O. Yurduseven, D. Smith, B. Livingstone, V. Schejbal, and Z. You, "Investigations of resolution limits for indirect microwave holographic imaging," Int. J. RF and Microwav. Computer-Aided Eng., vol. 23, vo. 4, pp. 410–416, July 2013.

[14] R. K. Amineh, N. K. Nikolova, M. Ravan, *Real-Time Three-Dimensional Imaging of Dielectric Bodies Using Microwave/Millimeter Wave Holography*. Wiley-IEEE Press, 2019.

[15] R. K. Amineh, J. McCombe, A. Khalatpour, N. K. Nikolova, "Microwave holography using point-spread functions measured with calibration objects," *IEEE Trans. Inst. and Meas.*, vol. 64, no. 2, pp. 403−417, 2015.

[16] R. K. Amineh, M. Ravan, A. Khalatpour, N. K. Nikolova, "Three-dimensional near-field microwave holography using reflected and transmitted signals," *IEEE Trans. Antennas Propag.*, vol. 59, no. 12, pp. 4777−4789, 2011.

[17] R. K. Amineh, M. Ravan, R. Sharma, and S. Baua, "Three-dimensional holographic imaging using single frequency microwave data," *Int. J. of Antennas and Propagation*, vol. 2018, Article ID 6542518, 14 pages, 2018.

[18] Ultra Wide band UWB+1S Antenna 2.8 GHz - 11 GHz for UWB TX/RX SDR RADAR GPR SIGINT EMC TEST ADSB WIFI FVP DRONE VIDEO VIVALDI ANTENNA Manufacturer: SMAKN, Amazon.com: SMAKN: Electronics

[19] K. He, J. Sun, and X. Tang, "Guided image filtering," *IEEE Trans. Pattern Analysis and Machine Intelligence*, vol. 35, no. 6, pp. 1397−1409, Jun. 2013.